DMD Fast Forward. Published on May 16, 2019 as DOI: 10.1124/dmd.119.086967
This article has not been copyedited and formatted. The final version may differ from this version.

Plasma and liver protein binding of GalNAc conjugated siRNA

Sara. C. Humphreys[1*], Mai B. Thayer[1], Julie M. Lade[1], Bin Wu[2], Kelvin Sham[2], Babak Basiri[1], Yue Hao[3], Xin Huang[3], Richard Smith[1] and Brooke M. Rock[1]

[1]Pharmacokinetics and Drug Metabolism Department, Amgen Research, 1120 Veterans Boulevard, South San Francisco, CA, 94080, USA

[2]Hybrid Modality Engineering Department, Amgen Research, One Amgen Center Drive, Thousand Oaks, CA, 91320, USA

[3]Molecular Engineering Department, Amgen Research, 360 Binney Street, Cambridge, MA, 02141, USA

*Corresponding author

DMD Fast Forward. Published on May 16, 2019 as DOI: 10.1124/dmd.119.086967
This article has not been copyedited and formatted. The final version may differ from this version.

Running Title: Plasma and liver protein binding of GalNAc-conjugated siRNA

Corresponding Author: Sara C. Humphreys

Department of Pharmacokinetics and Drug Metabolism, 1120 Veterans Boulevard, South San Francisco, 94080, CA, USA

Ph: (650)244-2471

shumph01@amgen.com

Number of text pages: 34

Number of tables: 2

Number of figures: 5

Number of references: 54

Number of words in Abstract: 174

Number of words in Introduction: 574

Number of words in Discussion: 1425

List of nonstandard abbreviations:

ASGPR - asialoglycoprotein receptor

ASO – antisense oligonucleotide

BLI – biolayer interferometry

f_u – fraction unbound

$f_{u,liver}$ – fraction unbound in liver homogenate

$f_{u,plasma}$ – fraction unbound in plasma

GalNAc - N-Acetylgalactosamine

MWCO – molecular weight cut-off

pAb – polyclonal antibody

PK-PD – pharmacokinetic-pharmacodynamic

PPB – plasma protein binding

R_h – hydrodynamic radius

DMD Fast Forward. Published on May 16, 2019 as DOI: 10.1124/dmd.119.086967
This article has not been copyedited and formatted. The final version may differ from this version.

ABSTRACT

Understanding siRNA fraction unbound (f_u) in relevant physiological compartments is critical for establishing pharmacokinetic-pharmacodynamic relationships for this emerging modality. In our attempts to isolate the equilibrium free fraction of GalNAc-conjugated siRNA using classical small molecule *in vitro* techniques, we observed that hydrodynamic radius was critical in determining the size exclusion limit requirements for f_u isolation; largely validating the siRNA 'rigid rod' hypothesis and providing insight into size-based kidney and lymphatic filtration of these molecules. With this knowledge, we developed an orthogonally-validated 50 kDa MWCO ultrafiltration assay to quantify f_u in biological matrices including human, non-human primate, rat, mouse plasma, and human liver homogenate. To enhance understanding of the siRNA-plasma interaction landscape, we examined the effects of various common oligonucleotide therapeutic modifications to the ribose and helix backbone on siRNA $f_{u,plasma}$ and found that chemical modifications can modulate plasma protein binding by at least 20%. Finally, to gain insight into which specific plasma proteins bind to siRNA, we developed a qualitative screen to identify binding “hits” across a panel of select purified human plasma proteins.

DMD Fast Forward. Published on May 16, 2019 as DOI: 10.1124/dmd.119.086967
This article has not been copyedited and formatted. The final version may differ from this version.

INTRODUCTION

Fraction unbound (f_u) is a measure of free drug at equilibrium in a biological matrix of interest. In this paper, we describe methods to quantify small interfering RNA (siRNA) f_u in plasma ($f_{u,plasma}$; commonly referred as plasma protein binding (PPB)) and liver tissue homogenate ($f_{u,liver}$). f_u is routinely quantified for small molecule therapeutic candidates according to the free drug hypothesis, wherein only the unbound fraction of drug is available to exhibit pharmacologic effects (Rowland et al. 2011). However, the role, if any, of f_u on the pharmacokinetic/pharmacodynamic (PK-PD) relationship has yet to be established for therapeutic siRNA.

siRNA is a rapidly emerging therapeutic modality, with the first US Food and Drug Administration (FDA) approval granted in August 2018 (Hoy 2018). Although oligonucleotide therapeutics like siRNA are generally treated as small molecules for regulatory filings, the FDA has not issued any specific guidance around the reporting of in vitro ADME properties (e.g. PPB) on this modality to date. While $f_{u,plasma}$ has been described for antisense oligonucleotide (ASO) therapeutics using 30 kilodalton (kDa) molecular-weight cut-off (MWCO) ultrafiltration, a corresponding assay has not yet been described for siRNA (Watanabe et al. 2006). For small molecules, $f_{u,plasma}$ is typically measured via ultracentrifugation, ultrafiltration or equilibrium dialysis. In these assays, the molecular size, shape, mass, and/or density of the small molecule relative to the plasma protein milieu largely determine its differential partitioning based on sedimentation velocity (ultracentrifugation) or porous membrane exclusion limits (ultrafiltration and equilibrium dialysis). For siRNA f_u isolation, the larger size of siRNA (approximately 15kDa with tri-antennary N-Acetylgalactosamine (GalNAc) conjugation) needed to be taken into consideration.

In this publication, we report an orthogonally-validated 50 kilodalton (kDa) molecular-weight cut-off (MWCO) ultrafiltration assay to quantify $f_{u,plasma}$ and $f_{u,liver}$ of a therapeutic siRNA in human matrices at clinically relevant concentrations, and across relevant pre-clinical species ($f_{u,plasma}$ only). The 21-mer double-stranded siRNA used throughout the study, referred to as siRNA-X, is chemically modified RNA with phosphorothioate (PS) bonds, 2′ O-methyl (2′-OMe) and 2′ deoxy 2′-Fluoro (2′-F) ribose

DMD Fast Forward. Published on May 16, 2019 as DOI: 10.1124/dmd.119.086967
This article has not been copyedited and formatted. The final version may differ from this version.

modifications, and GalNAc conjugation. PS bonds replace specific phosphodiester bonds to increase exonuclease resistance (Braasch et al. 2004), 2′-OMe and 2′-F enhance both stability and RNA-induced silencing complex (RISC) interactions (Choung et al. 2006, Allerson et al. 2005) and GalNAc enables targeted hepatocyte uptake via the asialoglycoprotein receptor (ASGPR) (Springer et al. 2018, Janas et al. 2018, Foster et al. 2018). siRNA-X is highly efficacious, eliciting greater than 80% target mRNA and protein knockdown over at least three months after a single 3 mg/kg dose in non-human primates (manuscript in preparation). Numerous chemical modifications and ligands employed in the current generation of oligonucleotide therapeutics, namely antisense oligonucleotide therapeutics (ASOs) have been demonstrated to alter the extent of protein binding (Wilce et al. 2012, Bailey et al. 2017, Geary et al. 2015, Juliano 2016, Bhandare et al. 2016, Schirle et al. 2016, Gaus et al. 2018). To understand how RNA modifications and ligand conjugation affect siRNA PPB specifically, we investigated the effects of PS, 2′-OMe, 2′-F, GalNAc and biotin on $f_{u,plasma}$.

Protein-siRNA interactions may affect siRNA tissue clearance, macroscopic (tissue-level) and microscopic (cell-level) distribution, and/or pharmacological activity; conversely, binding of siRNA to certain proteins may change the function or fate of those proteins. Taken together, these works addressing both total siRNA-matrix interactions to inform the former, and screening for specific siRNA-protein interactions to inform the latter, provide a set of complementary tools to begin to establish the role and the relevance of protein binding for this emerging modality. Furthermore, while the extent of total PPB at equilibrium is of interest from a PK-PD modeling perspective, knowledge of interactions between therapeutic siRNA and specific plasma proteins may help identify potential off-target protein-binding liabilities, drug-drug interactions, and aid design of next-generation siRNA molecules.

DMD Fast Forward. Published on May 16, 2019 as DOI: 10.1124/dmd.119.086967
This article has not been copyedited and formatted. The final version may differ from this version.

MATERIALS AND METHODS

Materials

All oligonucleotides were synthesized in-house using commercially available reagents or purchased from Integrated DNA Technologies (Skokie, IL). Human plasma proteins (albumin (#A3782), α-1-acid glycoprotein (#G9885), α-2-macroglobulin (#SRP6314), fibronectin (#F2006), fibrinogen (#F3879), haptoglobin (#372022), IgG Fc fragment (#AG714)) buffer reagents and Amicon Ultra 0.5 mL centrifugal filters (30 kDa MWCO (#UFC503008) and 50 kDa MWCO (#UFC505008)) were obtained from Millipore Sigma (Burlington, MA). Slide-A-Lyzer 0.5 mL MINI Dialysis Devices (20 kDa MWCO; #88402) were obtained from Thermo Fisher (Waltham, MA). α-thrombin was obtained from MP Biomedicals (Santa Ana, CA; #02194918). All plasma (K2 EDTA treated) and liver tissues were obtained from BioIVT (Westbury, NY). All plasma samples were from frozen pooled, mixed-gender donors. from: CD-1 mouse (MSEPLEDTA2; 300 donors), cynomolgus monkey (CYNPLEDTA2; 22 donors), sprague dawley rat (RATPLEDTA2; 60 donors), and human (HMPLEDTA2; 69 donors). Human liver tissue was from three pooled female donors (aged 30-40 years) and homogenized (from frozen) in Tissue Extraction Reagent I (Invitrogen #FNN071). Blocking reagents were sourced as follows: heparin (#84020), bovine serum albumin (#A9418), gelatin (#9000-70-8), 3-[(3-Cholamidopropyl)dimethylammonio]-1-propanesulfonate hydrate (aterials; #C3023) and spermidine (#S2626) were from Sigma (St. Louis, MO); I-Block™ (#T2015) was from Invitrogen (Carlsbad, CA), Tween-20 (#85113), Blocking Reagent (#11096176001), and Triton X-100 (#28314) were from Thermo Fisher. siRNA-specific rabbit polyclonal (pAb) antibody was generated by Lampire Biological Laboratories (Encinitas, CA) by immunization of rabbits with siRNA-X.

DMD Fast Forward. Published on May 16, 2019 as DOI: 10.1124/dmd.119.086967
This article has not been copyedited and formatted. The final version may differ from this version.

Methods

Time to equilibrium of siRNA binding to human plasma by bio-later interferometry

Biotinylated siRNA (biotin conjugated to the 3′ terminus of the sense strand; bn-siRNA) in Buffer A (10 mM Tris (pH 7.4), 150 mM NaCl, 1 mM $CaCl_2$ 1% gelatin (w/v), 0.13% Triton X-100 (w/v)) was loaded onto pre-equilibrated high precision streptavidin bio-sensors (ForteBio LLC, Fremont, CA) to obtain a response of ~1 nm over 1000 seconds. bn-siRNA-loaded tips were rinsed in Buffer A for one minute, followed by exposure to a five point (plus two blanks), 3-fold dilution series of human plasma in Buffer A (top concentration: 3.3% human plasma in Buffer A (v/v)) over 10 min. Data were collected on a ForteBio Octet-384 instrument, and analysis and fitting were performed using the ForteBio software (v10.0).

$f_{u,plasma}$ *and* $f_{u,liver}$ *determination by ultrafiltration*

To prepare the Ultracel® regenerated cellulose filters for use, residual glycerin was removed by twice adding 0.5 mL phosphate-buffered saline (PBS; 137 mM NaCl, 2.7 mM $CaCl_2$, 10 mM Na_2HPO_4, 1.8 mM KH_2PO_4 (pH 7.4) and spinning in a bench-top centrifuge for 10 min. at 3,000 ×*g*. Remaining PBS was removed before adding 0.5 mL PBS with 0.1% Tween-20 (w/v; PBST) and repeating the spin to prevent non-specific binding of drug to the filter. PBST was removed from the filter and collection tube immediately prior to sample addition (take care to avoid drying the filter). Samples were prepared by spiking known siRNA or small molecule concentrations into neat plasma or tissue homogenate (pre-equilibrated to 37°C) and incubated at 37°C for 30 minutes, shaking at 500 rpm. 500 µL sample was transferred into prepared filters and spun at 1,500 ×*g* until no more than 20% of the volume had passed through the filter. Only a small volume of ultrafiltrate should be collected, as the protein concentration in the upper reservoir rises during the filtration process (Zeitlinger et al. 2011). To mitigate matrix effects, after ultrafiltration, all donor samples were pre-treated with an equivalent volume of PBST, and all ultrafiltrate receiver samples were pre-treated with an equivalent volume of plasma/homogenate (standard curves were treated the same way). To measure recovery, drug-spiked PBST controls were performed at every concentration tested. During method development, we set an arbitrary cut-off of

DMD Fast Forward. Published on May 16, 2019 as DOI: 10.1124/dmd.119.086967
This article has not been copyedited and formatted. The final version may differ from this version.

80% recovery in buffer at each concentration tested to ensure that the corresponding f_u readout in plasma or homogenate was representative of the majority of siRNA in the sample. Ultracentrifugation and equilibrium dialysis methods are provided in the Supplemental Methods.

siRNA Detection and Quantitation via 96-well Plate-Based Hybridization Assay

Sheep pAb anti-digoxigenin antibody (Roche, #11222089001) was conjugated with a ruthenium label using the MSD Gold Sulfo-Tag NHS-Ester conjugation kit (Meso Scale Diagnostics™, #R31AA-1). Standards and sample buffer were made as follows: 10 mM Tris-HCl (pH 8.0) and 1 mM EDTA. Hybridization buffer was made as follows: 60 mM Na2PO4 [(pH 7.0, dibasic), 1 M NaCl, 5 mM EDTA, and 0.02% Tween 20. Lyophilized oligonucleotide probes were custom synthesized from Qiagen Inc. (Hilden, Germany). Sequence specific capture and detection probes were conjugated to biotin and digoxygenin, respectively. All chemicals and reagents were analytical grade or higher, if not specified.

Test article standard curves were prepared in PBS or plasma at a concentration range of 2.6-166 pM (0.04-2500 ng/mL). The standard curves and samples were diluted 1:10 in sample buffer and added to a 96-well PCR plate to a final volume of 50 µL. Both sequence specific capture and detection probes were added to hybridization buffer to a final concentration of 50 nM and 50 µL added to the samples in buffer. Sample and probes were hybridized in a thermal cycler under the following conditions: 90°C for 5 min., 35°C for 30 min., and a final hold at 12°C. After hybridization, samples were transferred to an MSD GOLD 96-well Streptavidin SECTOR PR plate (Meso Scale Diagnostics™, #L13SA) for 30 min. at room temperature. Plates were washed and incubated for 1 hour with 50 µL of 2 µg/mL ruthenium labeled anti-digoxygenin antibody in SuperBlock T20 TBS Blocking Buffer (Thermo Fisher, #37536). After a final wash, 150 µL of MSD Read Buffer T (Meso Scale Diagnostics™, #R92TD) was added and the plate was read in an MSD Sector S 600 instrument (Rockville, MD, USA).

Quantitation was performed against standard curves by non-liner regression (4PL) using GraphPad Prism (v7.04). For ultrafiltration and equilibrium dialysis, % recovery in buffer was calculated using Equation 1:

DMD Fast Forward. Published on May 16, 2019 as DOI: 10.1124/dmd.119.086967
This article has not been copyedited and formatted. The final version may differ from this version.

$$\%\, recovery\ (buffer) = \frac{[receiver]}{[donor]} \times 100 \quad \textbf{1}$$

where [donor] is the concentration of siRNA in buffer before addition to the apparatus, and [receiver] is the concentration of siRNA recovered in the ultrafiltrate, or on the other side of the dialysis membrane, respectively. f_u was calculated using Equation 2:

$$f_u = \frac{[receiver]}{[donor]} \quad \textbf{2}$$

Dilution of human liver tissue in homogenization buffer was accounted for using Equation 3 (Kalvass et al. 2007):

$$undiluted\ f_u = \frac{1/D}{1/f_{u,measured} - 1/D} \quad \textbf{3}$$

where *D* is the dilution factor.

Comparative LC-MS/MS analysis of small molecule $f_{u,plasma}$ and $f_{u,liver}$ via ultracentrifugation and ultrafiltration

LC-MS/MS was used to quantify post-50 kDa MWCO ultrafiltration and ultracentrifugation of warfarin, antipyrine, and timolol in human plasma, and rosuvastatin in human liver homogenate (see Supplementary Methods for ultracentrifugation $f_{u,plasma}$ *and* $f_{u,liver}$ method). Samples were quenched with 40% acetonitrile in water and spun for 10 minutes at 4,000 ×*g* before injection on a Kinetex C18 column (2.6 µm, 50 x 2.1 mm; Phenomenex) using a Shimadzu ultrafast-liquid chromatography system coupled to an AB Sciex Qtrap 4500 mass spectrometer with a source temperature of 550°C and an ion spray voltage of 4500 V. The mobile phases consisted of 0.1% formic acid in water (mobile phase A) and 0.1% formic acid in acetonitrile (mobile phase B) using a flow rate of 1 mL/min and a gradient as follows: 5% B for 0.8 min, 99% B for 0.5 min, and returned to 5% B to 1.5 min. Analytes were detected in positive ion mode using multiple reaction monitor monitoring (Q1→Q3; collision energy,

DMD Fast Forward. Published on May 16, 2019 as DOI: 10.1124/dmd.119.086967
This article has not been copyedited and formatted. The final version may differ from this version.

V): warfarin (309.0→163.0 m/z; 20 V), timalol (317.0→261.1 m/z; 25 V), antipyrine (189.1→161.1 m/z; 25 V), rosuvastatin (482.4→258.1 m/z; 45 V) and internal standard (IS) tolbutamide (309.0→163.0 m/z; 25 V). Compound peak areas were integrated using Analyst 1.6.2 software and normalized to the internal standard.

Binding of select purified human plasma proteins to biotinylated siRNA-X ± GalNAc

Binary siRNA-protein binding interactions were performed on the BLI with biotin-conjugated siRNA immobilized on streptavidin tips. 100 nM biotinylated siRNA-X (bn-siRNA-X) with or without GalNAc in Buffer A were loaded onto streptavidin BLI tips over 10 min. to ~2 nm. Loaded tips were rinsed in buffer for one minute, then introduced to 1:2 titrations of pAb anti-siRNA antibody (positive control), α-2-macroglobulin, α-thrombin, fibrinogen, fibronectin, albumin, α1-acid glycoprotein, α1-antitrypsin, haptoglobin, and IgG Fc fragment, starting at 1 μM (except the pAb anti-siRNA antibody control at 0.2 μM, and α-2-macroglobulin, α-thrombin, fibrinogen, fibronectin at 0.5 μM). Association and dissociation steps were performed for 10 minutes each.

DMD Fast Forward. Published on May 16, 2019 as DOI: 10.1124/dmd.119.086967
This article has not been copyedited and formatted. The final version may differ from this version.

RESULTS

Time to equilibrium and quasi-kinetic binding analysis using biolayer interferometry

f_u determination requires that the system be at equilibrium (Schmidt et al. 2010). BLI was used to measure the time taken for biotin-conjugated siRNA-X loaded onto streptavidin tips to reach steady state (Fig. 1). We observed that time-to-steady-state decreased with increasing plasma concentrations, and at 3.3% plasma, the system approached equilibrium in 10 minutes. Based on this result, and LC-MS evidence that siRNA-X is stable in plasma for more than 30 minutes (Supplemental Fig. 1) we determined that 30 minutes was sufficient for accurate f_u determination in neat plasma. It is important to recognize that for all PPB experiments, small molecules included, a compromise must be made to balance time-to-equilibrium with metabolic stability. Given that the rate of equilibration depends on the ligand-protein complex half-life ($t_{1/2}$; (Corzo 2006)), the sensorgrams do not appear to be approaching zero in the dissociation phase, and that plasma is a highly heterogeneous mixture of proteins, it is possible that a population of plasma proteins that bind siRNA tightly have not reached equilibrium in 30 minutes. Therefore, to ensure reproducibility, it is essential to perform the experiment with strict adherence to the 30 minutes equilibration time and temperature (37°C).

Comparison of classical small molecule PPB methods to determine the unbound fraction of siRNA in plasma

At roughly 15 kDa, GalNAc-conjugated siRNA is significantly larger than a typical SM. Consequently, isolation of the unbound fraction by a semi-permeable physical barrier (ultrafiltration and equilibrium dialysis) or by differential sedimentation (ultracentrifugation) requires some adaption from small molecule f_u isolation methods. Initially, we tested ultrafiltration and equilibrium dialysis devices with 30 and 20 kDa MWCO exclusion limits, respectively, based on commercial availability of devices with MWCOs close to, but greater than, 15 kDa. For ultracentrifugation, owing to complexities of achieving differential sedimentation of similarly sized macromolecular species (Hughes et al. 1938), we elected to test our existing ultracentrifugation small molecule protocol unmodified. We ran initial tests in protein-free medium to ensure that siRNA could freely diffuse across the semi-permeable membrane

DMD Fast Forward. Published on May 16, 2019 as DOI: 10.1124/dmd.119.086967
This article has not been copyedited and formatted. The final version may differ from this version.

(ultrafiltration and equilibrium dialysis) or would remain in the supernatant after spinning (ultracentrifugation).

Table 1 shows representative % recoveries of 1 μM siRNA-X in PBST in the receiver compartment (ultrafiltration and equilibrium dialysis) or supernatant (ultracentrifugation) for the three techniques. The recoveries– 0.0062%, 5.5%, and 24.8% for ultracentrifugation (small molecule method), equilibrium dialysis (20 kDa MWCO) and ultrafiltration (30 kDa MWCO), respectively – were too low for use in siRNA-f_u determination. At first, we hypothesized that the poor recovery was due to non-specific surface binding to filters, dialysis membranes and ultracentrifugation tubes. We explored a range of potential blocking reagents including heparin, alternative siRNA molecules, bovine serum albumin, gelatin, I-Block™, spermidine, Blocking Reagent, and Triton X-100. None of the blocking agents tested improved recovery over PBST, and several of them, including heparin, alternative siRNA, and spermidine, significantly reduced the sensitivity of the hybridization detection assay, potentially due to charge-based competition for the capture and detection probes. We subsequently discovered that the pore size of the permeable membrane was the largest determinant for recovery, as we recovered 92% of 1 μM siRNA-X in the receiver compartment of a filtration device with a 50 kDa MWCO in PBST. While this recovery represented a great improvement compared to where we started, with further optimization of blocking reagents, filter blocking routines, centrifugation speeds, recovery can be further improved. We did investigate the effect of replacing PBST with PBS with 0.1% CHAPS (w/v) and found that it significantly improved recovery of asymmetric (larger R_h) GalNAc-siRNA molecules (Supplemental Fig. 2). It is important to note that Watanabe et al. reported over 90% recovery of a fully phosphorothioated 20-mer DNA ASO using a 30 kDa MWCO ultrafiltration method (Watanabe et al. 2006), highlighting that ssDNA and dsRNA likely differ significantly in their structural conformations.

Akin to ultracentrifugation approaches to measure small molecule f_u, the ultrafiltration technique described here is likely subject to minor equilibrium perturbation effects as a consequence of the extent and duration of centrifugal force applied. siRNA-protein interactions most affected by this are weak

DMD Fast Forward. Published on May 16, 2019 as DOI: 10.1124/dmd.119.086967
This article has not been copyedited and formatted. The final version may differ from this version.

binders. To ensure reproducible and comparable results using this technique, we recommend using the centrifugation speeds and times described here.

Validation of siRNA R_h via calculation from literature values and siRNA-X crystal structure

After observing that a 50 kDa MWCO exclusion limit was required for adequate recovery of siRNA-X across an ultrafiltration apparatus in buffer (Table 1), we realized that R_h and not MW governs filter selection (these filters are typically designed for protein-based applications).

siRNA R_h can be calculated using helical rise per base-pair from literature values describing dsRNA A-form helix dimensions (Supplemental Calculations 1; (Taylor et al. 1985, Baeyens et al. 1995)). Initially, we were concerned that backbone and ribose modification of siRNA might cause deviations from the A-form helix structure, however, a crystal structure of siRNA-X confirmed the “rigid rod” linear geometry of siRNA, as well as the A-form helix (helical rise: 0.26-0.29 nm/base pair; R_h: ~2.7-3 nm; Fig. 2B; manuscript in preparation) Consequently, we used literature values of known protein R_h vs. protein MW to establish a correction factor to determine siRNA-protein MW equivalence (Fig. 6; R_h calculations shown in Supplemental Calculations 2). 21-mer siRNA-X is roughly equivalent to a 48 kDa protein, which is why it requires a 50 kDa MWCO filter.

Orthogonal validation of a 50 kDa MWCO ultrafiltration method for siRNA-X f_u determination using EMSA and LC-MS

Increasing the ultrafiltration MWCO from 30 kDa to 50 kDa resulted in a significant buffer recovery increase leading us to realize the importance of using of siRNA hydrodynamic radius (R_h) rather than molecular weight (MW) in determining which device to use for f_u determination (Table 1). However, given that human plasma consists of a highly heterogeneous mixture of proteins, many of which are 50 kDa or less, it was important to test whether the "unbound fraction" of siRNA in the receiver compartment of the ultrafiltration device was the true f_u or a mixture of unbound siRNA and siRNA bound to small proteins. We ran an electrophoretic mobility shift assay (EMSA) on the ultrafiltrate of 1 μM siRNA-X spiked into human plasma and observed two bands - one consistent with siRNA-X, the

DMD Fast Forward. Published on May 16, 2019 as DOI: 10.1124/dmd.119.086967
This article has not been copyedited and formatted. The final version may differ from this version.

other consistent with albumin (Supplemental Fig. 3A). Further testing of the albumin band in plasma without siRNA-X showed that albumin, or some compound that co-migrates with albumin, stains with SYBR Gold (Supplemental Fig. 3B); we later demonstrate that albumin does not bind siRNA-X using BLI (Supplemental Fig. 6). Together, these findings suggest that the clear majority of siRNA-X that passes through the 50 kDa MWCO filter is unbound.

Next, to determine whether the 50 kDa MWCO ultrafiltration method was a reliable measure of f_u, we tested it on a panel of small molecules with well-established $f_{u,plasma}$ and $f_{u,liver}$ values ranging from majority-bound (warfarin) to majority unbound (antipyrine). Table 2 provides a comparison of the reference f_u values obtained using classic PPB methods, compared to the 50 kDa MWCO ultrafiltration method. Warfarin $f_{u,plasma}$ was over-estimated approximately 4-fold. This is likely because warfarin binds to albumin, and we showed with EMSA that some fraction of albumin is recovered in the receiver compartment using the 50 kDa MWCO filter (Supplemental Fig. 3; the manufacturer also only reports >95% bovine serum albumin retention on these devices(http://www.emdmillipore.com/US/en/life-science-research/protein-sample-preparation/protein-concentration/amicon-ultra-centrifugal-filters/). Recovery of some quantity of albumin is expected given its high abundance and that its MW (~66 kDa) is sufficiently close to 50 kDa, and that the filter pore-sizes and represent a distribution at best and that albumin is not a perfect sphere. Rosuvastatin $f_{u,liver}$ ($f_{u,liver}$ = 0.14) was underestimated relative to the literature values ($f_{u,liver}$ = 0.23), which were generated using equilibrium dialysis (Pfeifer et al. 2013). This is likely because applying centrifugal force to homogenate results in blocking of the filtration pores to some extent. Lowering the centrifugation speed could minimize this effect, or this problem could be avoided entirely with equilibrium dialysis.

Cross-species comparison of siRNA PPB

As the development of therapeutic molecules necessitates testing in multiple preclinical species, it is important to understand if PPB properties are consistent across relevant species – in this case, mouse, rat, and cynomolgus monkeys – as well as in humans over a range of therapeutically relevant concentrations. Cross-species PPB comparisons could help at least partly explain any observed

DMD Fast Forward. Published on May 16, 2019 as DOI: 10.1124/dmd.119.086967
This article has not been copyedited and formatted. The final version may differ from this version.

differences in PK profiles. A two-way analysis-of-variance (ANOVA) of the data in Figure 3A indicated that there was no significant distinction for siRNA-X $f_{u,plasma}$ across the species tested (P>0.05), but that there was an increase in the fraction unbound with increasing concentration from 0.037–1 μM (P<0.01). The latter is consistent with PPB data reported across multiple modalities (Schmidt et al. 2010). However, given the limited concentration range it cannot be determined if PPB is concentration-independent (linear), or concentration-dependent (non-linear), as both cases have been reported (Deitchman et al. 2018). It should be noted that Gaus et al. recently observed that plasma binding of a 50% phosphorothioated DNA/RNA duplex was ~19-fold higher in monkey plasma compared to humans (mouse and rat were intermediate) (Gaus et al. 2018). This remains an area of active research.

Determination of siRNA-X $f_{u,liver}$ in human liver tissue homogenate

Many siRNA molecules currently under investigation as therapeutics, including siRNA-X, are targeted to the liver via GalNAc conjugation, which enables delivery via ASGPR-mediated uptake. It was therefore of interest to measure the unbound fraction in the liver. For SM, $f_{u,liver}$ is typically measured by equilibrium dialysis (Pfeifer et al. 2013), however, in the absence of commercially available devices with ~50 kDa MWCO for siRNA, we adapted the plasma ultrafiltration method described above to human liver homogenate (Fig. 3B). For siRNA-X, $f_{u,liver}$ ranged from 0.018-0.051 over a therapeutically relevant concentration range (0.375-6 μM), indicating that it is mostly bound in human liver tissue and that binding was higher in liver homogenate compared to plasma. Over this concentration range, the data did not appear to be strictly linear.

The effect of chemical modifications and ligand-conjugates on siRNA PPB

To investigate the effect of different chemical modifications on siRNA PPB, we measured $f_{u,plasma}$ on constructs with the same siRNA-X sequence that had been modified to be entirely 2′-OMe, 2′-F, or PS modified (Fig. 4). Consistent with the literature, we observed that PS increases PPB, and 2′-OMe decreases PPB relative to the siRNA-X control (Braasch et al. 2004, Choung et al. 2006, Allerson et al. 2005, Gaus et al. 2018). There was no statistically significant difference between siRNA-X and

DMD Fast Forward. Published on May 16, 2019 as DOI: 10.1124/dmd.119.086967
This article has not been copyedited and formatted. The final version may differ from this version.

fully 2′-F siRNA $f_{u,plasma}$. We could not find evidence in the literature discussing the role of 2′-F in siRNA PPB differences, however, in certain ASO cases, 2′-F appears to confer increased specificity and/or affinity to select cytosolic proteins (Shen et al. 2015, Vickers et al. 2016). At 1 μM siRNA, the effects of PS and 2′-OMe appear informative from an siRNA therapeutic design perspective because alterations in the numbers of these modifications could significantly affect the PK profile of siRNA in the blood.

We also looked at the effect of siRNA ligand conjugation on PPB and found that removal of GalNAc increased protein binding, and biotin had no statistically significant effect compared to siRNA-X. The implications of these findings are that conjugating biotin to siRNA to as a functional handle does not affect PPB and that GalNAc may be important for reducing PPB interactions. Furthermore, while siRNA-X $f_{u,plasma}$ was slightly less than $f_{u,serum}$, this result was not statistically significant, indicating that the role of clotting factors in total PPB is minimal. In addition, we ran the same PPB assay on a panel of four other therapeutic candidate siRNA molecules with different sequences and similar modification patterns, and found that at 1 μM siRNA, $f_{u,plasma}$ varied between approximately 0.08 and 0.15, which was significantly less than the effects observed with more extreme modification patterns here (data not shown).

Qualitative determination of specific interactions between siRNA-X and select human plasma proteins

We utilized BLI to gain further insight into which specific plasma proteins bound to siRNA-X. We elected to compare binding in the presence and absence of GalNAc due to the observation of different trends in total plasma protein binding when GalNAc was present or absent in various constructs (Supplemental Fig. 4&5), and because siRNA-X PPB significantly increased when GalNAc was removed (Fig. 4). Selection criteria for panel inclusion was based on plasma abundance (albumin, IgG Fc fragment, fibrinogen, α-2-macroglobulin, α-1-antitrypsin,and haptoglobin (Anderson et al. 2002)), prior evidence of prominent small molecule or ASO drug-binding (albumin, α-1-acid

glycoprotein, α-2-macroglobulin (Watanabe et al. 2006, Brown et al. 1994, Srinivasan et al. 1995, Cossum et al. 1993)), or RNA aptamer binding precedence (fibronectin (Ulrich et al. 2002) and α-thrombin (Long et al. 2008)). An siRNA-specific rabbit pAb antibody was used as a positive control.

α-2-macroglobulin and α-thrombin bound to both siRNA-X constructs, while fibronectin and fibrinogen bound to bn-siRNA-X(-Gal) only (Fig. 5), and no binding was observed with albumin, α1-acid glycoprotein, α1-antitrypsin, haptoglobin, and IgG Fc (negative results provided in Supplemental Fig. 6).

DMD Fast Forward. Published on May 16, 2019 as DOI: 10.1124/dmd.119.086967
This article has not been copyedited and formatted. The final version may differ from this version.

DISCUSSION

We have described and validated an assay to measure the free fraction of GalNAc-siRNA in plasma and liver homogenate at equilibrium. The rationale for developing the assay was to gain insight into the protein-binding properties of therapeutic siRNA molecules to support PK-PD modeling efforts and to pre-empt any regulatory filing requests. Under the International Council for Harmonization of Technical Requirements for Pharmaceuticals for Human Use (ICH) and Food and Drug Administration (FDA) guidelines, therapeutic siRNA is generally treated as a small molecule, as there is no specific guidance for this emerging modality. Small molecule regulatory filings typically require in vitro PPB data for pre-clinical animals and humans (S3A Guidance on Toxicokinetics (https://www.fda.gov/downloads/Drugs/GuidanceComplianceRegulatoryInformation/Guidances/UCM519697.pdf) and M3(R2) Guidance on Nonclinical Safety Studies for the Conduct of Human Clinical Trials and Marketing Authorization for Pharmaceuticals (https://www.fda.gov/downloads/Drugs/GuidanceComplianceRegulatoryInformation/Guidances/UCM073246.pdf)). To our knowledge, while f_u methods have been described for heavily phosphorothioated single-stranded DNA-based ASOs, this is the first description of an siRNA assay (Watanabe et al. 2006, Braasch et al. 2004, Cossum et al. 1993).

siRNA R_h dictates f_u separation requirements

A major finding of this work was that MWCO exclusion limits, which are estimated from approximately spherical globular proteins, cannot be directly applied to siRNA for f_u experiments because siRNA R_h is ~2-fold greater than a protein of equivalent MW (Hass et al. 2014). Therefore, to ensure siRNA can diffuse freely across a porous membrane for f_u separation, filters must be selected based on R_h and not MW.

siRNA is hypothesized to exist as a “rigid rod” in solution due to the geometry of the dsRNA A-form helix (Kozielski et al. 2013, Dandekar et al. 2015, Kornyshev et al. 2013). We recently obtained a crystal structure of siRNA-X confirming its linear geometry (R_h = ~2.7-3 nm; manuscript in preparation), consistent with literature descriptions of unmodified dsRNA (~0.28 nm helical rise/base-pair or R_h~2.9

DMD Fast Forward. Published on May 16, 2019 as DOI: 10.1124/dmd.119.086967
This article has not been copyedited and formatted. The final version may differ from this version.

nm for 21-mer siRNA). As it tumbles freely in solution, 21-mer siRNA R_h is roughly equivalent to a 48 kDa protein (Kok et al. 1981, Wilkins et al. 1999). This conservative estimate does not account for terminally positioned triantennary GalNAc or cation concentration and identity (shown for DNA (Fujimoto et al. 1994). 2′-F, 2′-OMe and PS modifications likely do not alter the A-form helical properties (Smith et al. 2000, Liu et al. 2011). Consequently, our recovery data (Table 1) support the siRNA rigid rod hypothesis.

An important implication of siRNA R_h elucidation is that certain organs in the body, including the kidney and lymph nodes, use filtration as a means of sorting molecules. Based on our findings we recommend using R_h-corrected MW to aid predictions of how these tissues process siRNA.

Application of protein binding data to interpret PK-PD profiles

PPB and liver protein binding f_u values for siRNA-X at equilibrium are not particularly informative in isolation as they do not address interaction dynamics and binding affinities in whole blood or at the site of action (e.g. liver). The true value of f_u measurements lies in how they can be applied to interpret the corresponding in vivo PK and PD data. Typical serum half-lives for GalNAc-siRNA range from 2-8 hours; in contrast, target mRNA knockdown can last from weeks to months (Nair et al. 2017). Such rapid clearance from blood would suggest that a majority of the observed 85-95% siRNA-X bound to proteins at equilibrium is only transiently bound with rapid dissociation rates (k_{off}). Consequently, if siRNA-X exhibits high affinity for any plasma proteins at all, these hypothetical proteins could only exist at low concentrations (<<37 nM the lowest PPB concentration tested). An important implication of this scenario is that tightly-bound siRNA-X could compete with endogenous ligands or otherwise interfere with physiological processes of low abundance plasma proteins.

As the GalNAc-siRNA chemistry repertoire continues to evolve, we advocate that the relationship between PPB and blood PK continue to be monitored, as changes in the identities of GalNAc-siRNA protein-binding partners and/or their affinities could lead to alterations in the distribution and exposure of the molecule, or adverse effects due to interference with endogenous processes. Moreover,

DMD Fast Forward. Published on May 16, 2019 as DOI: 10.1124/dmd.119.086967
This article has not been copyedited and formatted. The final version may differ from this version.

understanding the blood distribution, including protein binding partners, may be beneficial in defining strategies for extrahepatic delivery.

High affinity ASO binding to specific plasma proteins (nM; via fluorescence polarization) has directly impacted PD in knock-out (α-2-macroglobulin) or knock-down (histidine-2-glycoprotein) mice (Shemesh et al. 2016, Gaus et al. 2018). In both cases, protein removal from circulation resulted in 2-fold ASO activity increase, suggesting protein binding can modulate shunting to unproductive pathways. Although outside the scope of this paper, this experimental approach will aid understanding of the impact of protein binding on siRNA PD.

Given that GalNAc-siRNA is delivered to the liver via rapid ASGPR uptake, understanding siRNA-protein interactions at the site of action may aid understanding of the long duration of response. Our findings indicate siRNA is highly bound in the liver at equilibrium. If the binding turns out to be high-affinity, this could confirm the existence of a protein-bound 'depot' – with gradual release of siRNA to RISC. Other prevailing theories suggest that the 'depot' is a sub-cellular organelle like the endosome (Juliano et al. 2015, Dominska et al. 2010), or a consequence of RISC-mediated RNAi being a catalytic process with a long-lived Ago2-siRNA or Ago2-antisense complex (Wang et al. 2009, Okamura et al. 2004, Nakanishi 2016). Consequently, the contribution of liver protein binding to GalNAc-siRNA remains an open question.

Towards siRNA PPB engineering

Aligned with other published oligonucleotide data, our structure-activity relationship (SAR) data suggests that siRNA PPB is "tunable" (Watanabe et al. 2006, Cossum et al. 1993, Braasch et al. 2004) (Fig. 4). In our limited study looking at the effect of various common chemical modifications, we established that $f_{u,plasma}$ is manipulatable from 0.01-0.21 f_u at minimum. Whether binding modulation alters pharmacologic outcome remains to be seen. Modulation strategies might include minimizing binding to toxicity-related proteins, reducing drug-drug interaction liabilities, or targeting binding to specific proteins to facilitate siRNA delivery. For example, diacyl-conjugated siRNA displaying albumin-binding demonstrated increased circulation half-life compared to non-conjugated siRNA

DMD Fast Forward. Published on May 16, 2019 as DOI: 10.1124/dmd.119.086967
This article has not been copyedited and formatted. The final version may differ from this version.

(Sarett et al. 2017). More generally, therapeutics directly conjugated to albumin or IgG-containing moieties have prolonged circulatory half-lives due to engagement with the recycling neonatal Fc receptor and reduced kidney filtration (Larsen et al. 2018, Robbie et al. 2013). Other siRNA features currently under investigation that could be exploited for protein binding modulation include linker chemistry and conjugation to lipophilic molecules, peptides, monoclonal antibodies, or siRNA oligomers (Khan et al. 2016, Gandioso et al. 2017, Smith and Nikonowicz 2000, Tushir-Singh 2017).

Developing a standardized assessment of what makes a specific siRNA-protein interaction 'meaningful,' and characterizing protein-siRNA interactions in terms of specificity and affinity remains an active area of research. While we demonstrated that surfaced-based binding assays have utility in qualitatively identifying siRNA-binding partners (Fig. 5) we also observed significant orientation effects that are likely steric-driven (Supplemental Fig. 4&5). In future, to better rank-order molecules by binding affinity, solution-based equilibrium measurements such as fluorescence polarization (recently applied to ASOs (Gaus et al. 2018)) or kinetic exclusion assays are recommended. To identify novel binders, rather than use a bottom-up approach like the one performed here using purified proteins of interest, siRNA-protein pull-down combined with MS proteomics will provide a non-biased, comprehensive assessment of the siRNA-protein binding landscape. To delineate complex relationships between siRNA structure, protein binding, and pharmacological effect, additional studies addressing variation in sequence, chemical modification, modification pattern, and conjugation ligands are needed.

siRNA-protein interactions: Changing the binding paradigm in a therapeutic context

siRNA-protein interactions depend upon numerous factors including protein structure, siRNA sequence and chemical modifications, kinetics, and concentration. In biological matrices, additional considerations include competition with other proteins for siRNA binding, and competition with other oligonucleotides for protein binding, apply. Affinities between chemically-modified therapeutic oligonucleotides and specific proteins range from low nM to >500 μM (Gaus et al. 2018). Due to these complexities, siRNA-protein interactions are not well understood, and they cannot currently be

anticipated *a priori.* To advance siRNA therapeutics, a paradigm-shift in experimental design and interpretation is needed.

Rather than conforming to small molecule-like “lock and key” or “induced fit” principles (Koshland 1995), or protein-protein interactions where a certain threshold of specificity and stability is required to achieve meaningful binding (Vishwanath et al. 2017), siRNA-protein interactions are governed by multiple weak complementary forces. These forces are effectively enhanced by the high surface area and high surface area-to-density ratio of siRNA relative to other therapeutic modalities. They include electrostatic and hydrophobic interactions, hydrogen bonding, and base stacking (Koh et al. 2011, Tolstorukov et al. 2004, Luscombe et al. 2001, Jayaram et al. 2004). The consequences are complex binding events arising from a convolution of association and dissociation rates, reflecting a distribution of local affinities driven by chemical modification pattern, GalNAc or other conjugate, 5′ phosphorylation state, or 3′ base identity, blurring boundaries of how we think about interaction specificity (Jankowsky et al. 2015). Thus, to advance understanding of siRNA-protein interactions in a therapeutic setting, establishment of a new metric of what constitutes a “relevant” binding event in the context of PK-PD analysis is required.

A central rationale guiding us in this work has been to address the question “Does PPB matter for therapeutic siRNA?” In establishing an f_u assay to measure siRNA PPB and liver protein binding, and in developing an siRNA-protein interaction screening platform, we have established a bioanalytical toolkit to build out knowledge in this under-studied domain. In future, the *in vitro* techniques described here can aid *in vivo* PK-PD data interpretation for this emerging modality and guide design of the next generation of siRNA therapeutics.

ACKNOWLEDGEMENTS

Thank you to Christina Shen, Ben Jiang, Yun Ling, Zhican Wang, Justin Murray, and Fang Xie for their work supporting aspects of this project.

AUTHORSHIP CONTRIBUTIONS

Participated in research design: Humphreys, S.C., Rock, B.M., Lade, J.M., Thayer, M.B. and R. Smith

Conducted experiments: Humphreys, S.C., Lade, J.M., Basiri, B., Hao, Y. and X. Huang

Contributed new reagents or analytic tools: Wu, B. Sham, K., Thayer, M.B., Basiri, B., Hao, Y. and X. Huang

Performed data analysis: S.C. Humphreys

Wrote or contributed to the writing of the manuscript: Humphreys, S.C., Thayer, M.B., Rock, B.M. and R. Smith

REFERENCES

Allerson, C. R., N. Sioufi, R. Jarres, T. P. Prakash, N. Naik, A. Berdeja, L. Wanders, R. H. Griffey, E. E. Swayze & B. Bhat (2005) Fully 2'-Modified Oligonucleotide Duplexes with Improved in Vitro Potency and Stability Compared to Unmodified Small Interfering RNA. *Journal of Medicinal Chemistry,* 48**,** 901-904.

Anderson, N. L. & N. G. Anderson (2002) The Human Plasma Proteome. *Molecular & Cellular Proteomics,* 1**,** 845.

Baeyens, K. J., H. L. De Bondt & S. R. Holbrook (1995) Structure of an RNA double helix including uracil-uracil base pairs in an internal loop. *Nature Structural Biology,* 2**,** 56.

Bailey, J. K., W. Shen, X.-H. Liang & S. T. Crooke (2017) Nucleic acid binding proteins affect the subcellular distribution of phosphorothioate antisense oligonucleotides. *Nucleic acids research,* 45**,** 10649-10671.

Bhandare, V. & A. Ramaswamy (2016) Structural Dynamics of Human Argonaute2 and Its Interaction with siRNAs Designed to Target Mutant tdp43. *Advances in bioinformatics,* 2016**,** 8792814-8792814.

Braasch, D. A., Z. Paroo, A. Constantinescu, G. Ren, O. K. Öz, R. P. Mason & D. R. Corey (2004) Biodistribution of phosphodiester and phosphorothioate siRNA. *Bioorganic & Medicinal Chemistry Letters,* 14**,** 1139-1143.

Brown, D. A., S. H. Kang, S. M. Gryaznov, L. DeDionisio, O. Heidenreich, S. Sullivan, X. Xu & M. I. Nerenberg (1994) Effect of phosphorothioate modification of oligodeoxynucleotides on specific protein binding. *Journal of Biological Chemistry,* 269**,** 26801-26805.

Choung, S., Y. J. Kim, S. Kim, H.-O. Park & Y.-C. Choi (2006) Chemical modification of siRNAs to improve serum stability without loss of efficacy. *Biochemical and Biophysical Research Communications,* 342**,** 919-927.

Corzo, J. (2006) Time, the forgotten dimension of ligand binding teaching. *Biochem Mol Biol Educ,* 34**,** 413-6.

Cossum, P. A., H. Sasmor, D. Dellinger, L. Truong, L. Cummins, S. R. Owens, P. M. Markham, J. P. Shea & S. Crooke (1993) Disposition of the 14C-labeled phosphorothioate oligonucleotide ISIS 2105 after intravenous administration to rats. *Journal of Pharmacology and Experimental Therapeutics,* 267**,** 1181.

Dandekar, P., R. Jain, M. Keil, B. Loretz, M. Koch, G. Wenz & C. M. Lehr (2015) Enhanced uptake and siRNA-mediated knockdown of a biologically relevant gene using cyclodextrin polyrotaxane. *Journal of Materials Chemistry B,* 3**,** 2590-2598.

Deitchman, A. N., R. S. P. Singh & H. Derendorf (2018) Nonlinear Protein Binding: Not What You Think. *J Pharm Sci,* 107**,** 1754-1760.

Dominska, M. & D. M. Dykxhoorn (2010) Breaking down the barriers: siRNA delivery and endosome escape. *Journal of Cell Science,* 123**,** 1183.

Foster, D. J., C. R. Brown, S. Shaikh, C. Trapp, M. K. Schlegel, K. Qian, A. Sehgal, K. G. Rajeev, V. Jadhav, M. Manoharan, S. Kuchimanchi, M. A. Maier & S. Milstein (2018) Advanced siRNA Designs Further Improve In Vivo Performance of GalNAc-siRNA Conjugates. *Molecular Therapy,* 26**,** 708-717.

Fujimoto, B. S., J. M. Miller, N. S. Ribeiro & J. M. Schurr (1994) Effects of different cations on the hydrodynamic radius of DNA. *Biophys J,* 67**,** 304-8.

Gandioso, A., A. Massaguer, N. Villegas, C. Salvans, D. Sanchez, I. Brun-Heath, V. Marchan, M. Orozco & M. Terrazas (2017) Efficient siRNA-peptide conjugation for specific targeted delivery into tumor cells. *Chem Commun (Camb),* 53**,** 2870-2873.

Gaus, H. J., R. Gupta, A. E. Chappell, M. E. Ostergaard, E. E. Swayze & P. P. Seth (2018) Characterization of the interactions of chemically-modified therapeutic nucleic acids with plasma proteins using a fluorescence polarization assay. *Nucleic Acids Res*.

Geary, R. S., D. Norris, R. Yu & C. F. Bennett (2015) Pharmacokinetics, biodistribution and cell uptake of antisense oligonucleotides. *Advanced Drug Delivery Reviews,* 87**,** 46-51.

Hoy, S. M. (2018) Patisiran: First Global Approval. *Drugs*.

Hughes, T. P., E. G. Pickels & F. L. Horsfall (1938) A method for determining the differential sedimentation of proteins in the high speed concentration centrifuge. *The Journal of Experimental Medicine,* 67**,** 941.

Janas, M. M., M. K. Schlegel, C. E. Harbison, V. O. Yilmaz, Y. Jiang, R. Parmar, I. Zlatev, A. Castoreno, H. Xu, S. Shulga-Morskaya, K. G. Rajeev, M. Manoharan, N. D. Keirstead, M. A. Maier & V. Jadhav (2018) Selection of GalNAc-conjugated siRNAs with limited off-target-driven rat hepatotoxicity. *Nature Vommunications,* 9**,** 723-723.

Jankowsky, E. & M. E. Harris (2015) Specificity and nonspecificity in RNA-protein interactions. *Nat Rev Mol Cell Biol,* 16**,** 533-44.

Jayaram, B. & T. Jain (2004) The role of water in protein-DNA recognition. *Annu Rev Biophys Biomol Struct,* 33**,** 343-61.

Juliano, R. L. (2016) The delivery of therapeutic oligonucleotides. *Nucleic Acids Research,* 44**,** 6518-6548.

Juliano, R. L. & K. Carver (2015) Cellular uptake and intracellular trafficking of oligonucleotides. *Advanced drug delivery reviews,* 87**,** 35-45.

Kalvass, J. C., T. S. Maurer & G. M. Pollack (2007) Use of Plasma and Brain Unbound Fractions to Assess the Extent of Brain Distribution of 34 Drugs: Comparison of Unbound Concentration Ratios to in Vivo P-Glycoprotein Efflux Ratios. *Drug Metabolism and Disposition,* 35**,** 660.

Khan, T., H. Weber, J. DiMuzio, A. Matter, B. Dogdas, T. Shah, A. Thankappan, J. Disa, V. Jadhav, L. Lubbers, L. Sepp-Lorenzino, W. R. Strapps & M. Tadin-Strapps (2016) Silencing Myostatin Using Cholesterol-conjugated siRNAs Induces Muscle Growth. *Mol Ther Nucleic Acids,* 5**,** e342.

Koh, Y. Y., Y. Wang, C. Qiu, L. Opperman, L. Gross, T. M. Tanaka Hall & M. Wickens (2011) Stacking interactions in PUF-RNA complexes. *RNA,* 17**,** 718-27.

Kok, C. M. & A. Rudin (1981) Relationship between the hydrodynamic radius and the radius of gyration of a polymer in solution. *Die Makromolekulare Chemie, Rapid Communications,* 2**,** 655-659.

Kornyshev, A. A. & S. Leikin (2013) Helical structure determines different susceptibilities of dsDNA, dsRNA, and tsDNA to counterion-induced condensation. *Biophys J,* 104**,** 2031-41.

Koshland, D. E. (1995) The Key–Lock Theory and the Induced Fit Theory. *Angewandte Chemie International Edition in English,* 33**,** 2375-2378.

Kozielski, K. L., S. Y. Tzeng & J. J. Green (2013) Bioengineered nanoparticles for siRNA delivery. *Wiley interdisciplinary reviews. Nanomedicine and nanobiotechnology,* 5**,** 449-468.

Larsen, M. T., H. Rawsthorne, K. K. Schelde, F. Dagnaes-Hansen, J. Cameron & K. A. Howard (2018) Cellular recycling-driven in vivo half-life extension using recombinant albumin fusions tuned for neonatal Fc receptor (FcRn) engagement. *J Control Release,* 287**,** 132-141.

Liu, J., S. Guo, M. Cinier, L. S. Shlyakhtenko, Y. Shu, C. Chen, G. Shen & P. Guo (2011) Fabrication of Stable and RNase-Resistant RNA Nanoparticles Active in Gearing the Nanomotors for Viral DNA Packaging. *ACS Nano,* 5**,** 237-246.

Long, S. B., M. B. Long, R. R. White & B. A. Sullenger (2008) Crystal structure of an RNA aptamer bound to thrombin. *RNA,* 14**,** 2504-2512.

Luscombe, N. M., R. A. Laskowski & J. M. Thornton (2001) Amino acid-base interactions: a three-dimensional analysis of protein-DNA interactions at an atomic level. *Nucleic Acids Res,* 29**,** 2860-74.

Nair, J. K., H. Attarwala, A. Sehgal, Q. Wang, K. Aluri, X. Zhang, M. Gao, J. Liu, R. Indrakanti, S. Schofield, P. Kretschmer, C. R. Brown, S. Gupta, J. L. S. Willoughby, J. A. Boshar, V. Jadhav, K. Charisse, T. Zimmermann, K. Fitzgerald, M. Manoharan, K. G. Rajeev, A. Akinc, R. Hutabarat & M. A. Maier (2017) Impact of enhanced metabolic stability on pharmacokinetics and pharmacodynamics of GalNAc-siRNA conjugates. *Nucleic Acids Res,* 45**,** 10969-10977.

Nakanishi, K. (2016) Anatomy of RISC: how do small RNAs and chaperones activate Argonaute proteins? *Wiley interdisciplinary reviews. RNA,* 7**,** 637-660.

O'Reilly, R. A. (1972) Sodium warfarin. *Pharmacology,* 8**,** 181-90.

Okamura, K., A. Ishizuka, H. Siomi & M. C. Siomi (2004) Distinct roles for Argonaute proteins in small RNA-directed RNA cleavage pathways. *Genes & development,* 18**,** 1655-1666.

Pfeifer, N. D., K. B. Harris, G. Z. Yan & K. L. Brouwer (2013) Determination of intracellular unbound concentrations and subcellular localization of drugs in rat sandwich-cultured hepatocytes compared with liver tissue. *Drug Metab Dispos,* 41**,** 1949-56.

Robbie, G. J., R. Criste, W. F. Dall'acqua, K. Jensen, N. K. Patel, G. A. Losonsky & M. P. Griffin (2013) A novel investigational Fc-modified humanized monoclonal antibody, motavizumab-YTE, has an extended half-life in healthy adults. *Antimicrob Agents Chemother,* 57**,** 6147-53.

Rowland, M., T. N. Tozer & M. Rowland. 2011. *Clinical pharmacokinetics and pharmacodynamics : concepts and applications*. Philadelphia: Wolters Kluwer Health/Lippincott William & Wilkins.

Sarett, S. M., T. A. Werfel, L. Lee, M. A. Jackson, K. V. Kilchrist, D. Brantley-Sieders & C. L. Duvall (2017) Lipophilic siRNA targets albumin in situ and promotes bioavailability, tumor penetration, and carrier-free gene silencing. *Proc Natl Acad Sci U S A,* 114**,** E6490-E6497.

Schirle, N. T., G. A. Kinberger, H. F. Murray, W. F. Lima, T. P. Prakash & I. J. MacRae (2016) Structural Analysis of Human Argonaute-2 Bound to a Modified siRNA Guide. *Journal of the American Chemical Society,* 138**,** 8694-8697.

Schmidt, S., D. Gonzalez & H. Derendorf (2010) Significance of protein binding in pharmacokinetics and pharmacodynamics. *J Pharm Sci,* 99**,** 1107-22.

Shemesh, C. S., R. Z. Yu, H. J. Gaus, P. P. Seth, E. E. Swayze, F. C. Bennett, R. S. Geary, S. P. Henry & Y. Wang (2016) Pharmacokinetic and Pharmacodynamic Investigations of ION-353382, a Model Antisense Oligonucleotide: Using Alpha-2-Macroglobulin and Murinoglobulin Double-Knockout Mice. *Nucleic Acid Ther,* 26**,** 223-35.

Shen, W., X. H. Liang, H. Sun & S. T. Crooke (2015) 2'-Fluoro-modified phosphorothioate oligonucleotide can cause rapid degradation of P54nrb and PSF. *Nucleic Acids Res,* 43**,** 4569-78.

Smith, J. S. & E. P. Nikonowicz (2000) Phosphorothioate Substitution Can Substantially Alter RNA Conformation. *Biochemistry,* 39**,** 5642-5652.

Springer, A. D. & S. F. Dowdy (2018) GalNAc-siRNA Conjugates: Leading the Way for Delivery of RNAi Therapeutics. *Nucleic Acid Therapeutics,* 28**,** 109-118.

Srinivasan, S. K., H. K. Tewary & P. L. Iversen (1995) Characterization of Binding Sites, Extent of Binding, and Drug Interactions of Oligonucleotides with Albumin. *Antisense Research and Development,* 5**,** 131-139.

Taylor, P., F. Rixon & U. Desselberger (1985) Rise per base pair in helices of double-stranded rotavirus RNA determined by electron microscopy. *Virus Research,* 2**,** 175-182.

Tolstorukov, M. Y., R. L. Jernigan & V. B. Zhurkin (2004) Protein-DNA hydrophobic recognition in the minor groove is facilitated by sugar switching. *J Mol Biol,* 337**,** 65-76.

Tushir-Singh, J. (2017) Antibody-siRNA conjugates: drugging the undruggable for anti-leukemic therapy. *Expert Opinion on Biological Therapy,* 17**,** 325-338.

Ulrich, H., M. H. Magdesian, M. J. M. Alves & W. Colli (2002) In Vitro Selection of RNA Aptamers That Bind to Cell Adhesion Receptors of Trypanosoma cruzi and Inhibit Cell Invasion. *Journal of Biological Chemistry,* 277**,** 20756-20762.

Vickers, T. A. & S. T. Crooke (2016) Development of a Quantitative BRET Affinity Assay for Nucleic Acid-Protein Interactions. *PLoS One,* 11**,** e0161930.

Vishwanath, S., A. Sukhwal, R. Sowdhamini & N. Srinivasan (2017) Specificity and stability of transient protein-protein interactions. *Curr Opin Struct Biol,* 44**,** 77-86.

Wang, H.-W., C. Noland, B. Siridechadilok, D. W. Taylor, E. Ma, K. Felderer, J. A. Doudna & E. Nogales (2009) Structural insights into RNA processing by the human RISC-loading complex. *Nature structural & molecular biology,* 16**,** 1148-1153.

Watanabe, T. A., R. S. Geary & A. A. Levin (2006) Plasma protein binding of an antisense oligonucleotide targeting human ICAM-1 (ISIS 2302). *Oligonucleotides,* 16**,** 169-80.

Wilce, J., J. Vivian & M. Wilce. 2012. Oligonucleotide Binding Proteins. In *Protein Dimerization and Oligomerization in Biology,* ed. J. M. Matthews, 91-104. New York, NY: Springer New York.

Wilkins, D. K., S. B. Grimshaw, V. Receveur, C. M. Dobson, J. A. Jones & L. J. Smith (1999) Hydrodynamic Radii of Native and Denatured Proteins Measured by Pulse Field Gradient NMR Techniques. *Biochemistry,* 38**,** 16424-16431.

Yoshikado, T., K. Toshimoto, T. Nakada, K. Ikejiri, H. Kusuhara, K. Maeda & Y. Sugiyama (2017) Comparison of Methods for Estimating Unbound Intracellular-to-Medium Concentration Ratios in Rat and Human Hepatocytes Using Statins. *Drug Metab Dispos,* 45**,** 779-789.

Zeitlinger, M. A., H. Derendorf, J. W. Mouton, O. Cars, W. A. Craig, D. Andes & U. Theuretzbacher (2011) Protein binding: do we ever learn? *Antimicrob Agents Chemother,* 55**,** 3067-74.

FOOTNOTES

Author Disclosures:

All authors are employees and stock holders of Amgen, Inc.

DMD Fast Forward. Published on May 16, 2019 as DOI: 10.1124/dmd.119.086967
This article has not been copyedited and formatted. The final version may differ from this version.

FIGURE LEGENDS

Figure 1: Representative time-to-equilibrium of siRNA binding to total human plasma. Reference tip-subtracted sensorgrams depicting a titration of total human plasma interacting with biotinylated siRNA on streptavidin tips. Top plasma concentration is 3.3% (v/v) in Buffer A followed by a 1:2 dilution series.

Figure 2: (A) Workflow of determination of siRNA f_u via ultrafiltration. Step 1: pre-treat filter with detergent-containing buffer (we found that PBST (Table 1) and PBS+CHAPS (Supplemental Fig. 2 provided good recovery with a 50 kDa MWCO filter). Step 2: add pre-equilibrated siRNA-spiked matrix into donor compartment of filter and centrifuge. Step 3: collect flow-though and quantify siRNA $f_{u.}$ (B) Depiction of siRNA-X R_h based off the crystal structure.

Figure 3: PPB and liver protein binding of siRNA-X. (A) Cross-species comparison of $f_{u,plasma}$ across a range of therapeutically relevant siRNA concentrations. There was a significant increase in $f_{u,plasma}$ with concentration ($P<0.01$) that was not dependent on species (determined by two-way ANOVA, GraphPad Prism) (B) siRNA-X $f_{u,liver}$ across a range of therapeutically relevant concentrations. Plasma measurements were performed in triplicate; liver measurements were performed in duplicate.

Figure 4: Effect of chemical modifications on $f_{u,plasma}$ at 1μM siRNA concentration. (A) Constructs tested with the sense strand depicted at the top (5′-3′) and the complementary antisense strand at the bottom. The RNA base sequence was constant across constructs, with only the conjugated ligand/s (GalNAc and biotin), the ribose (2′-OMe, 2′-F), and the backbone (PS or PO) changing. (B) $f_{u,plasma}$ for each of the constructs in plasma; siRNA-X was also measured in serum. Results were compared using an ordinary one-way ANOVA with multiple comparisons in GraphPad Prism. Significant differences between the test article, siRNA-X in plasma, and the other constructs are reported as * = $P<0.05$, ** = $P<0.01$, *** = $P<0.001$ and **** = $P<0.0001$.

DMD Fast Forward. Published on May 16, 2019 as DOI: 10.1124/dmd.119.086967
This article has not been copyedited and formatted. The final version may differ from this version.

Figure 5: BLI sensorgrams of positive screening hits for select human plasma proteins binding to biotinylated siRNA-X ± GalNAc. A side-by-side comparison of pAb anti-siRNA antibody (pAb; positive control), α-2-macroglobulin, α-thrombin, fibrinogen, and fibronectin binding to bn-siRNA-X with (left column) or without (right column) GalNAc conjugation. Titrations were 1:2 dilutions with a top conc. of 0.5 μM (except pAb = 0.2 μM).

Figure 6: The relationship between R_h and MW for globular proteins does not hold for the dsRNA linear polymer according to the R_h observed in the crystal structure. siRNA is marked in red. GalNAc was not included in the R_h calculation. Linear regression was performed on the protein subset to estimation of the MW for a protein with an equivalent R_h to siRNA. The equation of the line obtained (with siRNA omitted) was $y = 0.03509x + 1.233$ and this was used to calculate the siRNA-protein MW equivalence value of ~48 kDa (GraphPad Prism; calculations provided in Supplemental Calculations 2).

DMD Fast Forward. Published on May 16, 2019 as DOI: 10.1124/dmd.119.086967
This article has not been copyedited and formatted. The final version may differ from this version.

TABLES

Table 1: Comparison of % siRNA-X recovery using different f_u isolation techniques

f_u isolation method	***MWCO (kDa)***	***% recovery***
ultracentrifugation	n/a	0.0062 ± 0.0003
equilibrium dialysis	20	5.53 ± 7.13
ultrafiltration	30	24.7 ± 1.4
ultrafiltration	50	92.4 ± 11.6

DMD Fast Forward. Published on May 16, 2019 as DOI: 10.1124/dmd.119.086967
This article has not been copyedited and formatted. The final version may differ from this version.

Table 2: Validation of 50 kDa MWCO ultrafiltration method for determination of $f_{u,plasma}$ and $f_{u,liver}$ using well-characterized small molecules

SM	***matrix*** *(human)*	f_u (measured)	f_u (reference)	***Reference method***
antipyrine	plasma	0.867 ± 0.110	0.9	ultracentrifugation
timolol	plasma	0.347 ± 0.074	0.4	ultracentrifugation
warfarin	plasma	0.043 ± 0.007	0.01†	ultracentrifugation
rostuvastatin	liver homog.	0.14 ± 0.03	0.23‡	equilibrium dialysis

† *(O'Reilly 1972)*

‡ *(Yoshikado et al. 2017), (Pfeifer et al. 2013)*

DMD Fast Forward. Published on May 16, 2019 as DOI: 10.1124/dmd.119.086967
This article has not been copyedited and formatted. The final version may differ from this version.

FIGURES

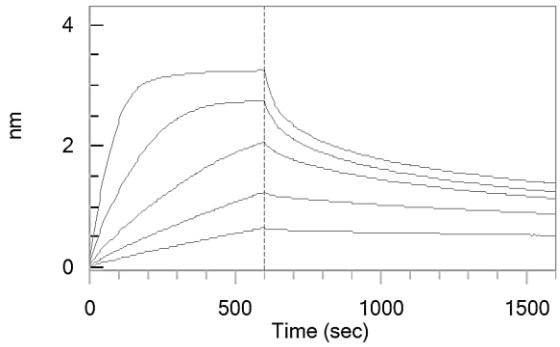

Figure 1

DMD Fast Forward. Published on May 16, 2019 as DOI: 10.1124/dmd.119.086967
This article has not been copyedited and formatted. The final version may differ from this version.

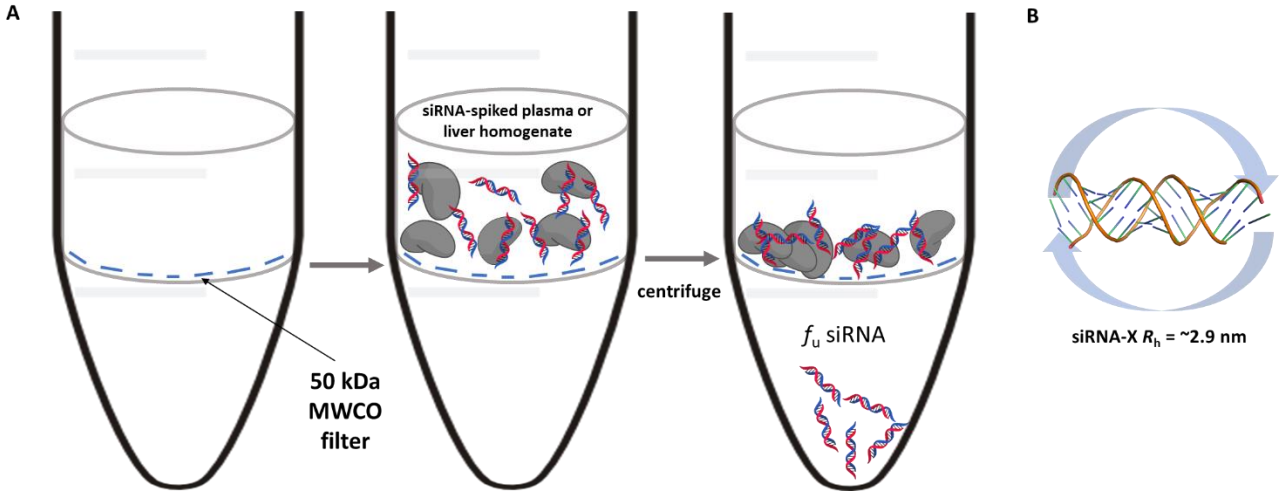

Figure 2

DMD Fast Forward. Published on May 16, 2019 as DOI: 10.1124/dmd.119.086967
This article has not been copyedited and formatted. The final version may differ from this version.

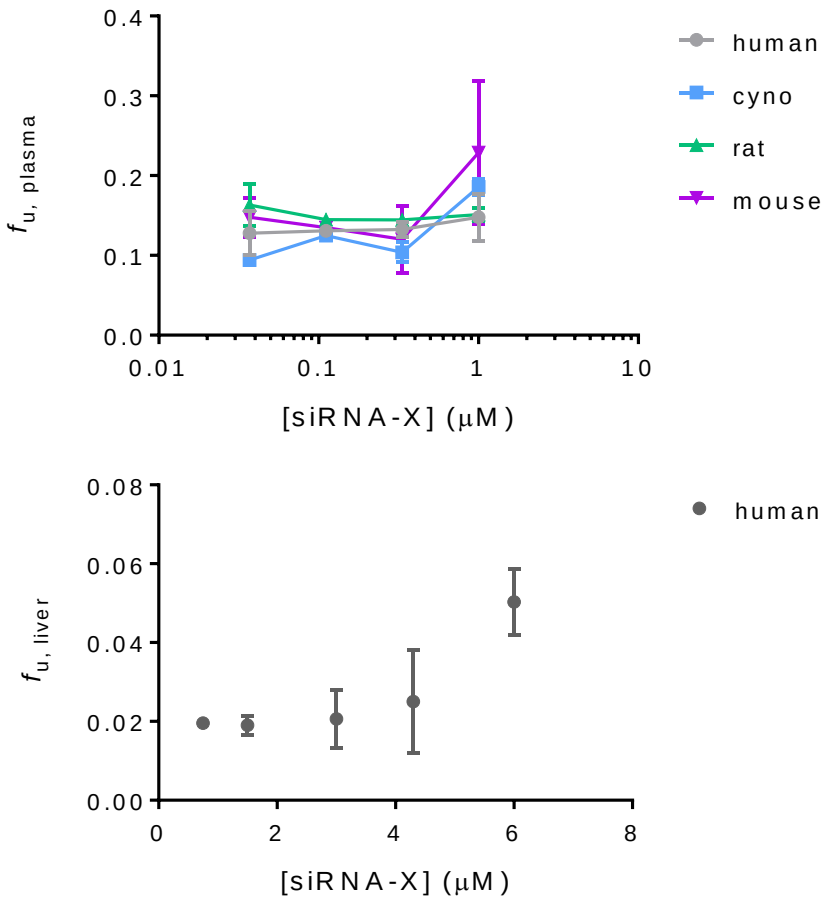

Figure 3

DMD Fast Forward. Published on May 16, 2019 as DOI: 10.1124/dmd.119.086967
This article has not been copyedited and formatted. The final version may differ from this version.

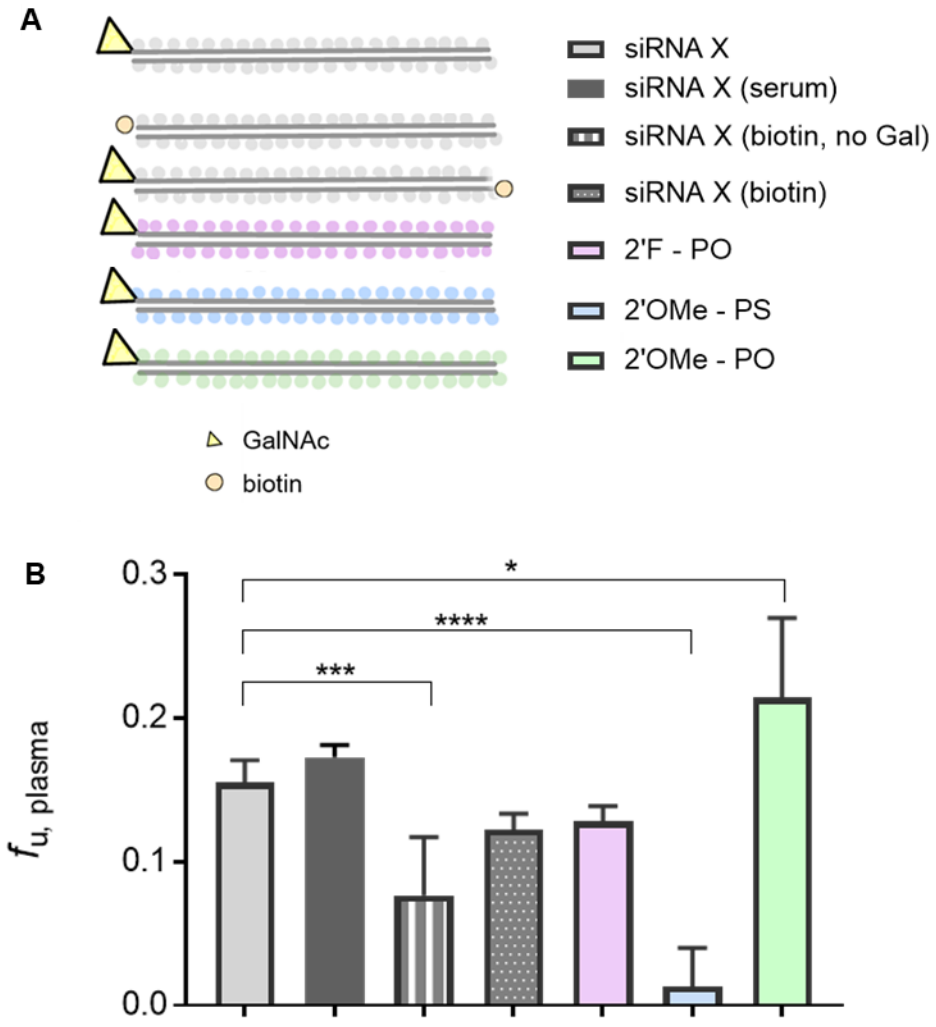

Figure 4

DMD Fast Forward. Published on May 16, 2019 as DOI: 10.1124/dmd.119.086967
This article has not been copyedited and formatted. The final version may differ from this version.

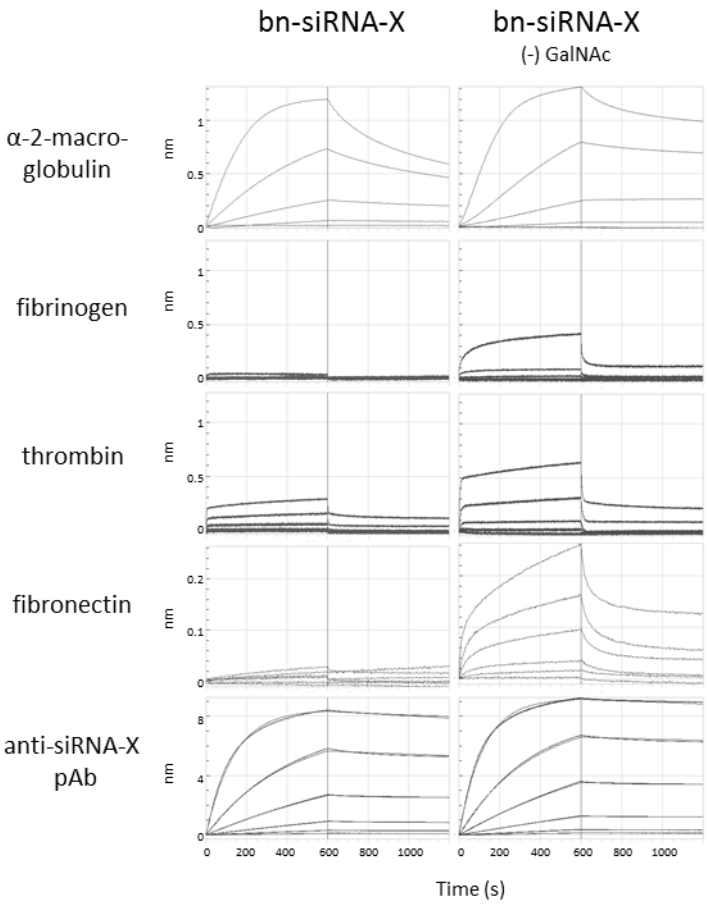

Figure 5

DMD Fast Forward. Published on May 16, 2019 as DOI: 10.1124/dmd.119.086967
This article has not been copyedited and formatted. The final version may differ from this version.

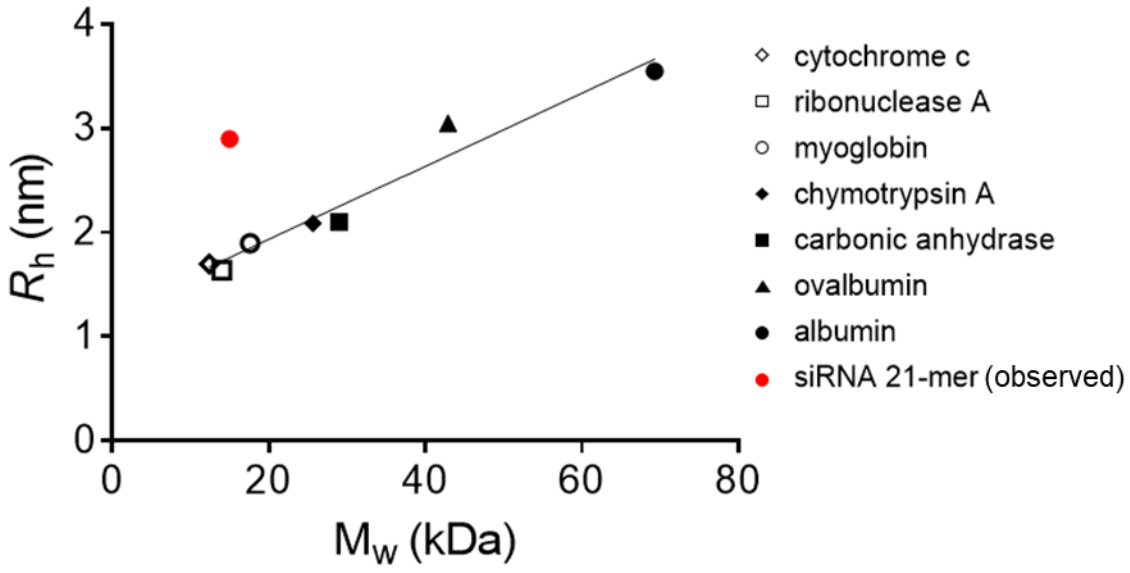

Figure 6